Quantum–Thermal Crossover of Hydrogen and Tritium Diffusion in α-Iron

ARTICLE *in* THE JOURNAL OF PHYSICAL CHEMISTRY C · NOVEMBER 2012

Impact Factor: 4.77 · DOI: 10.1021/jp307660e

THE JOURNAL OF PHYSICAL CHEMISTRY C

Article

pubs.acs.org/JPCC

Quantum–Thermal Crossover of Hydrogen and Tritium Diffusion in α-Iron

Takehiro Yoshikawa* and Toshiyuki Takayanagi*

Department of Chemistry, Saitama University, Shimo-Okubo 255, Sakura-ku, Saitama City, Saitama 338-8570, Japan

Hajime Kimizuka

Department of Mechanical Science and Bioengineering, Graduate School of Engineering Science, Osaka University, 1-3 Machikaneyama-cho, Toyonaka, Osaka 560-851, Japan

Motoyuki Shiga*

Center for Computational Science and E-systems, Japan Atomic Energy Agency, The University of Tokyo, 5-1-5, Kashiwanoha, Kashiwa City, Chiba 277-8563, Japan

ABSTRACT: The diffusion coefficients of hydrogen (H) and tritium (T) in α-Fe have been computed using two approximate quantum dynamical techniques, that is, centroid molecular dynamics (CMD) and ring polymer molecular dynamics (RPMD), in the temperature range of T = 100−1000 K using the embedded atom method (EAM) potential. It has been found that the RPMD and CMD methods give very similar results. From a further analysis based on quantum transition-state theory (centroid density QTST) combined with path integral molecular dynamics (PIMD), it has been clear that there is a crossover between thermal and quantum mechanisms at about T = 500 and 300 K for H and T diffusions, respectively. The importance of nuclear quantum effects at low temperatures has been illustrated in terms of the effective free-energy surface map.

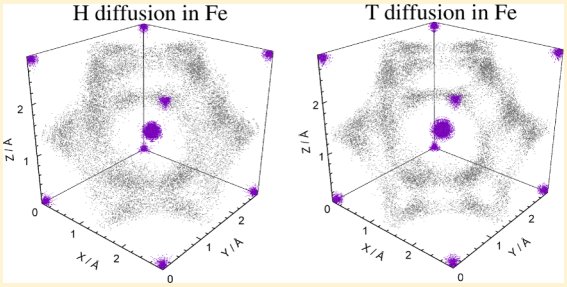

INTRODUCTION

Safe control of tritium is one of the technological challenges in the development of next-generation deuterium–tritium fusion reactors where tritium is used as nuclear fuel.[1,2] Tritium should be strictly confined to prevent from contamination by contacts to the external environment via isotopic exchange with hydrogen in water or hydrocarbons. However, the fundamental database for the properties of tritium that supports such investigations is far from being complete. For instance, the migration rates of tritium in metallic materials which constitute the reactor, as well as the underlying physics of migration, have not been discussed thoroughly from a scientific viewpoint. This status is highly in contrast to the case of hydrogen/deuterium migration, which has been a long-standing research field associated with scientific interest and technological problems such as hydrogen storage and hydrogen embrittlement.[3−6] The difference is presumably due to the experimental difficulty in dealing with strongly radioactive tritium. Thus, the computational approach would be an alternative that is free of such an experimental limitation. In particular, it is expected that molecular simulation is a useful way that has access to microscopic mechanisms on the atomistic level for a given form of interatomic forces, in principle.

In this paper, we investigate the rate and the mechanism of hydrogen (H) and tritium (T) diffusion in the α phase of iron (α-Fe). In addition to the technological importance of Fe and Fe alloys as major structural materials for nuclear reactor plants, it is pointed out that the diffusion coefficients of H in α-Fe are the highest among the values reported thus far for any metal,[7] and thus H interstitials in Fe are extremely mobile even at low temperatures. Detailed information on the behavior of H isotopes in Fe is important for understanding the fundamental processes of fast solid-state diffusion and transport in metal-H isotope systems. Previous studies on nonradioactive isotopes, H and deuterium (D) in Fe and other body-centered cubic (bcc) metals,[8−20] suggest the coexistence of thermal and quantum diffusion mechanisms, the former and the latter being dominant at high and low temperatures, respectively. In particular, very recently, Kimizuka et al.[18−20] have applied centroid molecular dynamics simulations including quantum mechanical nature of nuclei for the H atom diffusion processes in Fe. They found a curved non-Arrhenius behavior for the temperature dependence of the calculated diffusion coefficients below T ∼ 500 K

Received: August 2, 2012
Revised: September 12, 2012
Published: September 19, 2012

and concluded that quantum nature of H atoms is playing an essential role in diffusion mechanisms. Therefore, it is necessary to use a simulation method where both thermal and quantum diffusion processes are taken into account. For this purpose, we use two distinct methods based on the approximate quantum dynamics theories relevant to the imaginary time path integral formulation,[21−23] that is, centroid molecular dynamics (CMD),[24−30] and ring polymer molecular dynamics (RPMD).[31−34] It should be mentioned that the RPMD method has been recently applied to hydrogen atom diffusion on the Ni(100) surface.[35] We here compare the CMD and RPMD results with those from quantum transition-state theory (centroid density QTST),[17,36−40] where the free-energy barrier along the diffusive reaction path is estimated numerically by path integral molecular dynamics (PIMD). Moreover, we have also carried out classical molecular dynamics (classical MD) where quantum effect is switched off; that is, only the thermal effect is included. All of these simulations have been done systematically within the temperature range of T = 100−1000 K. We note that this is the first report on the quantum molecular dynamics simulation of T diffusion in metals, according to the authors' knowledge. It generally requires more computational effort to obtain the trajectory of T diffusion whose rate is much slower than H or D diffusion.

COMPUTATIONAL DETAILS

For the Fe−H interaction, we have used the embedded atom method (EAM) potential to describe the interaction among hydrogen/tritium in the bcc Fe lattice.[18,19] The EAM is an empirical implementation of effective medium theory for the binding energy of a metal,[42,43] which includes many-body effects. The energy of a system is given by

$$V = \frac{1}{2}\sum_{i=1,j\neq i}^{N}\varphi_{ij}(r_{ij}) + \sum_{i=1}^{N}F_i(\rho_i) \quad (1)$$

where the former term corresponds to pair interactions φ as a function of the distance r_{ij} between the atoms i and j, and the latter term is an atomic embedding energy F as a function of the local electron density ρ_i. Thus, the EAM potential for Fe−H is specified by seven functions: φ_{FeFe}, φ_{FeH}, φ_{HH}, F_{Fe}, F_H, ρ_{Fe}, and ρ_H. According to the EAM model in refs 18 and 19, we used the functions of φ_{FeFe}, F_{Fe}, and ρ_{Fe} that were developed by Mendelev et al.[44] and the functions of φ_{HH}, F_H, and ρ_H that were developed by Angelo et al.[45] For the function of φ_{FeH}, we used the model developed by Kimizuka et al.[18,19] with reference to work of Jiang and Carter.[46] The lattice constant l_c and dissolution energy E_s at the most stable structure of $Fe_{128}H$ obtained from this potential are 2.8553 Å and 0.20 eV (not including zero-point correction), respectively. The dissolution energy including zero-point vibrational energy is 0.30 eV.[46] Notice that the corresponding experiment values are 2.86 Å and 0.30 eV, respectively.[47] Therefore, our EAM potential energy interaction reasonably reproduces experimental physical quantities.

The geometry and potential energy profile of the Fe−H system obtained from this potential is presented in Figure 1a,b. The contour plot of the potential energy in Figure 1b is shown as a function of the H position on the (100) plane of the bcc Fe lattice. Notice that the four corners correspond to the Fe positions in the lattice. The most stable trapping site of H is located at the tetrahedral site (T-site, closed circle) and is at ($L \pm L/2$, L) and (L, $L \pm L/2$) of the (100) plane where $L = l_c/2$.

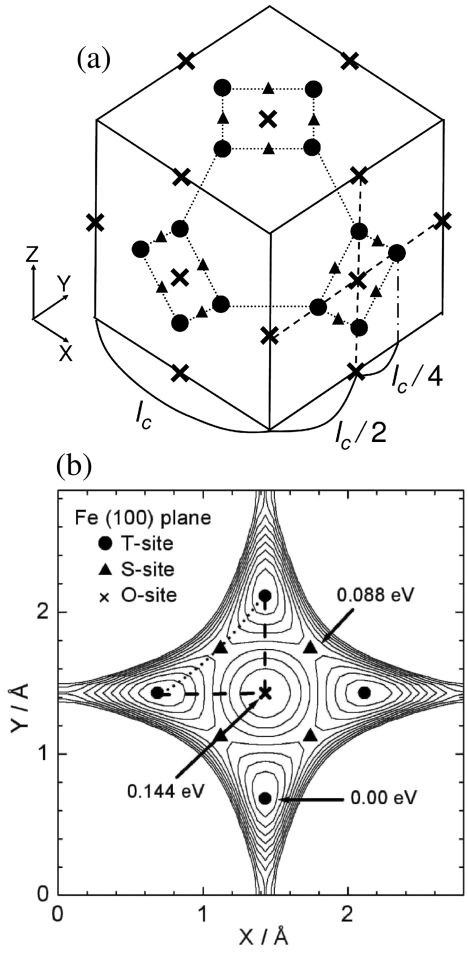

Figure 1. (a) Three-dimensional perspective plots of the stationary points and (b) two-dimensional potential energy surface as a function of Cartesian (X,Y) coordinates (in Å) obtained from the EAM interaction potential on the Fe(100) plane. Contour increments are set to 0.02 eV. Closed circles, closed triangle, and cross indicate T-site, S-site, and O-site, respectively. Dotted line represents the minimum energy path via the S-site, and broken line represents the diffusion pathway through the O-site.

The H diffusion microscopically consists of the migration of the H atom from one T-site to another neighboring T-site (dotted line). The saddle-point site (S-site, closed triangle) is a transition state for the H migration, which is located around the midpoint between the two neighboring T-sites. The energy of a H atom at the S-site is 0.088 eV higher than that at the T-site. The H atom diffusion may also occur through the octahedral site (O-site, cross), corresponding to the second-order saddle point on the potential energy surface. The O-site is at the center of the (100) plane. The energy state of the H atom at the O-site is lying at 0.144 eV above that at the T-site. These values are comparable with potential energy barriers obtained from density functional theory.[46] This suggests that the most energetically favorable diffusion pathway should be that from the T-site to the neighboring T-site via the S-site. However, notice that this simple idea cannot be applied when quantized zero-point vibrational energy is taken into account. Since the O-site corresponds to the second-order saddle point as mentioned above, it has two imaginary vibrational frequencies, while the S-site has only one imaginary vibrational frequency. This implies that the energy difference between the S-site and O-site may become significantly smaller when

dx.doi.org/10.1021/jp307660e | J. Phys. Chem. C 2012, 116, 23113−23119

Table 1. H/T Diffusion Coefficients (in 10^{-8} m^2 s^{-1}) in the Temperature Range of 100−1000 K in Fe (Statistical Errors Have Been Evaluated from the Standard Error with Respect to 15 Independent Trajectories in Each Condition)

T/K	hydrogen exp. (D_H/D_T)	CMD[a]	CMD	RPMD	classical	tritium CMD	RPMD	classical
100		0.43	0.36 ± 0.22	0.44 ± 0.10	NA	0.03 ± 0.02	0.03 ± 0.01	NA
200			0.55 ± 0.01	0.48 ± 0.01	(2.98 ± 0.04) × 10^{-2}	0.08 ± 0.02	0.07 ± 0.03	(1.78 ± 0.12) × 10^{-2}
300	0.74−0.87[b,c]/0.09[b,d]	0.83	0.83 ± 0.33	0.84 ± 0.24	0.32 ± 0.17	0.17 ± 0.07	0.18 ± 0.06	(13.1 ± 0.09) × 10^{-2}
500	1.5−1.7[b]	1.15	1.08 ± 0.15	1.24 ± 0.25	0.92 ± 0.13	0.64 ± 0.09	0.72 ± 0.15	0.60 ± 0.02
700	1.9−2.2[b]		1.75 ± 0.26	1.87 ± 0.05	1.92 ± 0.16	1.21 ± 0.12	1.19 ± 0.11	1.17 ± 0.12
800	2.0−2.4[b]		1.99 ± 0.12	1.95 ± 0.11	2.21 ± 0.06	1.33 ± 0.30	1.28 ± 0.15	1.25 ± 0.08
900			2.18 ± 0.08	2.04 ± 0.18	2.30 ± 0.02	1.55 ± 0.21	1.52 ± 0.10	1.41 ± 0.16
1000	2.45 − 2.63[b,e]	2.37	2.50 ± 0.16	2.32 ± 0.04	2.37 ± 0.11	1.56 ± 0.04	1.53 ± 0.15	1.58 ± 0.12

[a]Previous CMD results taken from refs 18 and 19. [b]Experimental data taken from refs 8−15 and 56. [c]Measured at 293 K. [d]Measured for tritium in Fe at 286 K. [e]Measured at 973 K.

quantized vibrational frequencies are taken into account. Interestingly, Kimizuka et al.[19] found that the two diffusion pathways for H through the S-site and O-site have comparable free-energy barriers at T = 100−200 K, while the diffusion pathway through the S-site becomes more important as temperature increases. Therefore, one should take into account the nuclear quantum effects in order to discuss the H/T diffusion processes in Fe more quantitatively.

In the imaginary time path integral formulation, the quantum statistics of the system composed of N atoms can be mapped to the classical statistics of NP particles having the effective potential

$$V_{\mathrm{eff}} = \sum_{i=1}^{N}\sum_{s=1}^{P}\frac{Pm_i}{2\beta^2\hbar^2}(\boldsymbol{x}_{i,s} - \boldsymbol{x}_{i,s-1})^2 + \frac{1}{P}\sum_{s=1}^{P}V(\boldsymbol{x}_{1,s}\ldots\boldsymbol{x}_{N,s}) \tag{2}$$

with the cyclic condition, $\boldsymbol{x}_{i,0} = \boldsymbol{x}_{i,P}$, where $\boldsymbol{x}_{i,s}$ is the position of the ith atom in the sth imaginary time slice (i.e., bead). This is isomorphic to a system of N harmonic ring polymers, each of which consists of P beads, which are interacting by the second term of eq 2, describing the bead average of the physical potential V. The harmonic interaction between the neighboring beads is given by a spring constant, $Pm_i/(2\beta^2\hbar^2)$, where m_i is the mass of the ith atom, and $\beta = 1/k_BT$ using the Boltzmann constant k_B and the temperature T. The CMD and RPMD are approximate quantum dynamical techniques in which the Kubo-transformed correlation function can be derived approximately from the dynamical trajectories on this effective potential. In the CMD approach, one solves the equation of motion of the centroid variables, $q_i = (1/P)\sum_{s=1}^{P}\boldsymbol{x}_{i,s}$, according to the average forces acting on $\boldsymbol{q}_i$, where the statistical average is taken with respect to the configurations of the noncentroid variables. In the RPMD approach, one solves the equation of motion of all beads $\boldsymbol{x}_{i,s}$ according to the forces acting on $\boldsymbol{x}_{i,s}$. Although the CMD and RPMD methods are quite distinct in concepts, their practical difference between them (and also between the PIMD methods) is simply in the way of setting the fictitious mass and thermostats for the temperature control.[48,49]

The diffusion constant of CMD/RPMD is given by the mean square displacement

$$D = \lim_{t\to\infty}\frac{1}{6t}\langle|\boldsymbol{q}_X(t) - \boldsymbol{q}_X(0)|^2\rangle \tag{3}$$

where the angular bracket denotes the statistical average obtained from the CMD/RPMD trajectory and X is the diffusive atom, H or T. In practice, the time interval t is chosen to be large such that the mean square displacement increases linearly in time.

It would be useful to compare these dynamical results with a simpler estimation by centroid density QTST based on the traditional QTST.[17,36−41,50,51] This approach assumes the stochastic process of crossing over the effective free-energy barrier in terms of the centroid coordinates

$$D_{\mathrm{QTST}}(T) = \upsilon(T)\exp(-\Delta F/k_BT) \tag{4}$$

where

$$\Delta F = -k_BT\log\frac{Q(\mathbf{q}_{\mathrm{TS}})}{Q(\mathbf{q}_{\mathrm{EQ}})} \tag{5}$$

ΔF is the free-energy difference between the transition state either at O- and S-site ($\boldsymbol{q}_{\mathrm{TS}}$) and equilibrium at T-site ($\boldsymbol{q}_{\mathrm{EQ}}$) associated with the quantum partition function for fixed centroid coordinates as

$$Q(\boldsymbol{q}) = \prod_{i=1}^{N}\left[\left(\frac{m_iP}{2\pi\beta\hbar^2}\right)^{3P/2}\int d\boldsymbol{x}_{i,1}\ldots\int d\boldsymbol{x}_{i,P}\right]\prod_{i=1}^{N}\left(\boldsymbol{q}_i - \frac{1}{P}\sum_{s=1}^{P}\boldsymbol{x}_{s,i}\right)\exp(-\beta V_{\mathrm{eff}}) \tag{6}$$

$\upsilon(T)$ is the pre-exponential factor which is weakly dependent on temperature in general. The PIMD simulation is able to provide $\exp(-\Delta F/k_BT)$ since it is equal to the ratio of the centroid probability distributions at the S-site (O-site) and T-site although the direct evaluation of $D_{\mathrm{QTST}}(T)$ is difficult from the PIMD simulation result. In this work, $\upsilon(T)$ is roughly estimated from the RPMD and CMD results and is used to discuss a crossover temperature below.[17]

For each temperature condition (100−1000 K), the PIMD simulation were carried out for 2000000 steps with a time increment Δt = 0.1 fs, which was enough to equilibrate the system. For the PIMD (CMD) runs, the Nóse-Hoover chain thermostats were attached to all of the degrees of freedom (the noncentroid degrees of freedom only) to control the temperature strongly. In all of the calculations, we have employed the $Fe_{128}H$ supercell under periodic boundary conditions (lattice constant l_c = 2.8553 Å and 4 × 4 × 4 unit cells). After some test calculations, we have chosen the number of beads to be P = 24−128 (24 for 1000 K and 128 for 100 K) which give converged results. Then, using those initial positions and velocities, the CMD and RPMD simulations were restarted with a time increment of Δt = 0.1 fs. For the CMD runs, the adiabaticity parameter γ was set to 0.1. The total step for each

dx.doi.org/10.1021/jp307660e | J. Phys. Chem. C 2012, 116, 23113−23119

CMD or RPMD trajectory was taken to be N_s = 4000000 (t = 0.4 ns) at each temperature. The final results were averaged over 15 independent trajectories for both the CMD and RPMD simulations. Since the RPMD dynamics does not use thermostats, one can employ a larger time step for RPMD simulations than that for CMD simulations.[52] In order to confirm this, we have carried out the RPMD calculations with larger time steps of Δt = 0.5 and 1.0 fs. As a result, we found that the obtained diffusion coefficients were comparable to that obtained with Δt = 0.1 fs. This suggests that the RPMD simulations are more efficient for obtaining a large number of trajectories than the CMD simulations. However, we here report computational results with Δt = 0.1 fs for both RPMD and CMD simulations since the final results were averaged over the same number of trajectories. The details of our computational code are also described in refs 53−55.

RESULTS AND DISCUSSION

First, we present the results of diffusion coefficients obtained from our simulations. Table 1 summarizes the diffusion coefficients of H and T (D_H and D_T) in Fe calculated with the CMD and RPMD methods at several temperatures in the range of T = 100−1000 K. We have also calculated the diffusion coefficients from classical MD simulations (i.e., with P = 1), and the corresponding results are also included in Table 1. The statistical error estimated from the standard deviation of diffusion coefficients was obtained from 15 independent trajectories. It can be seen that both CMD and RPMD results are in very good agreement within statistical uncertainty.[8−15] It is also found that the classical MD simulations give much smaller diffusion coefficients than the CMD and RPMD results at low temperatures, as expected, due to the lack of quantum mechanical tunneling. On the other hand, the classical MD results are close to the quantum ones of CMD/RPMD at high temperatures. In particular, the diffusion coefficients for T obtained from the classical MD agree well with both the CMD and RPMD values in the temperature range of T = 700−1000 K.

In the previous CMD work of Kimizuka et al.,[18,19] the H diffusion coefficients with the same EAM potential were in reasonable agreement with experimental measurements over the temperature range of T = 300−1000 K.[8−15] This suggests that both the CMD and RPMD simulations using the present EAM potential energy surface can give reliable estimates of diffusion coefficients for hydrogen. Therefore, it is suggested that the present CMD and RPMD simulations give reasonable diffusion coefficients also for tritium. As far as we are aware, there has been only one report on the experimental diffusion coefficients for T; Hagi and Hayashi have estimated the diffusion coefficients for T and H in Fe at T = 286 K to be D_T = 0.09×10^{-8} m^2 s^{-1} and D_H = 0.4×10^{-8} m^2 s^{-1} using an indirect electrochemical permeation method.[56] It seems that this value of H diffusion coefficient seems to be underestimated since it is almost one-half of our CMD and RPMD values ($0.83-0.84 \times 10^{-8}$ m^2 s^{-1} at T = 300 K) as well as other experimental values reported in the literature ($0.74-0.89 \times 10^{-8}$ m^2 s^{-1} at T = 300 K; see Table 1).[8−15] In general, measurements of diffusion coefficients in Fe−H system strongly depend on the purity of the specimen, that is, concentration of vacancies and impurities, while the specimen of Hagi and Hayashi contains somewhat more impurities (>0.1 mass %) than in other measurements.[8−15,56] Thus, it might be due to the trapping effects that the estimated tritium diffusion coefficient is underestimated in the study of Hagi and Hayashi.[56] Their experimental D_T value is also about one-half of our CMD, and RPMD calculations give D_T at T = 300 K to be 0.17×10^{-8} and 0.18×10^{-8} m^2 s^{-1}, respectively, although the temperature is slightly different from the experimental temperature. However, the ratio for D_T and D_H is in agreement between the computational and experimental results.

Figure 2a,b presents Arrhenius plots of the diffusion coefficients of H and T in Fe, respectively. The results of the

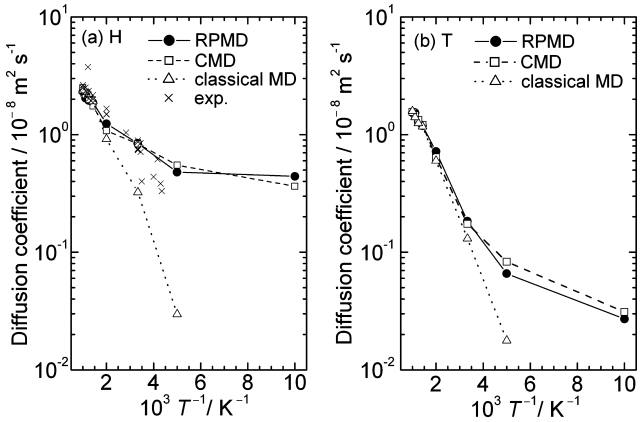

Figure 2. Arrhenius plots of the diffusion coefficients for hydrogen and tritium in Fe. Experimental data are taken from refs 8−15. Solid, broken, and dotted lines represent results of RPMD, CMD, classical MD simulations, respectively.

RPMD, CMD, and classical MD are shown by closed circles, open squares, and open triangles, respectively. The experimental data for H are presented with cross symbols in Figure 2a. The Arrhenius plots of the diffusion coefficients of both isotopes calculated with the classical MD method are almost on the straight lines within the temperature range considered here. On the other hand, the diffusion coefficients of both H and T obtained from the present quantum mechanical CMD and RPMD simulations show strong nonlinear behaviors at low temperatures. More specifically, a deviation from linearity begins around T = 500 K for H diffusion, while for T diffusion, a deviation can be seen below $T \sim$ 300 K (see Table 1). The former behavior is in excellent agreement with the previous CMD calculations of Kimizuka et al.[18,19] Similar results can be also observed in other metals and solids.[16−18,57−59] These results indicate that a nuclear quantum effect (i.e., quantum tunneling) is playing an essential role in the diffusion of H and T in Fe at low temperatures.

In order to understand the isotope effect for H and T diffusion in detail, we plot the ratio of the diffusion coefficients D_H/D_T as a function of $1000/T$ in Figure 3. It can be seen that both the CMD and RPMD methods give very similar curves within statistical uncertainty; D_H/D_T increases with the temperature decrease. The D_H/D_T value is seen to be nearly constant around 1.6−1.8 in the higher temperature range (>500 K). Notice that this value is close to the square root of the tritium−hydrogen mass ratio of 3.0, in agreement with the classical mechanics. In addition, this result is comparable with experiments in the range of error at room temperature.[8−15,56]

Figure 4 displays a representative three-dimensional perspective plot of the nuclear distribution function for the H/T (gray color) in Fe (purple color) obtained from the PIMD simulation at T = 300 K. In Figure 4a, a large fluctuation

dx.doi.org/10.1021/jp307660e | J. Phys. Chem. C 2012, 116, 23113−23119

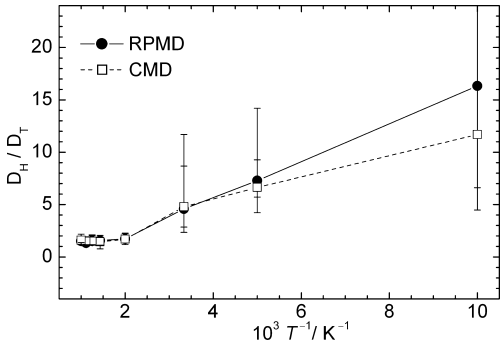

Figure 3. Ratio of the diffusion coefficients for hydrogen and tritium as a function of $1000/T$ obtained from the present CMD and RPMD simulations.

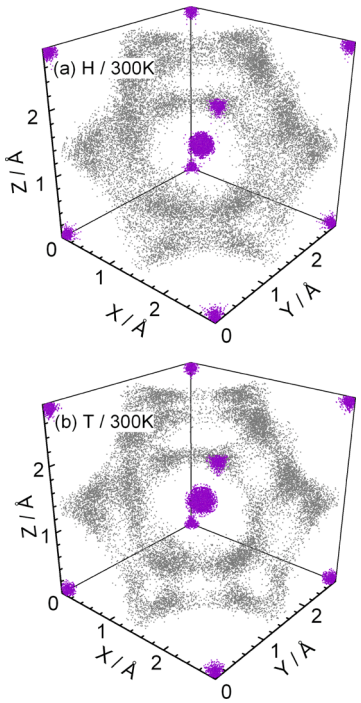

Figure 4. Three-dimensional perspective plots of nuclear distribution of (a) Fe−H and (b) Fe−T obtained from the PIMD simulations at T = 300 K. The purple color represents the iron atoms, and the gray color represents the hydrogen or tritium. The T-sites are at $(L \pm L/2, L)$ and $(L, L \pm L/2)$ of the (100) plane where $L = l_c/2$, and the O-site is at the center of the (100) plane.

can be seen for a H atom. In particular, we can see that the hydrogen is distributed around not only the paths between T-sites via S-sites but also around the O-sites. In Figure 4b, however, motion of T is clearly different from H atoms, and distributions of T around the O-site are much less than those of H. This clearly shows that there is a significant difference in the mechanisms of H and T diffusions on the ability to pass through the O-site. On the other hand, the spread of spatial distribution for the Fe atoms is relatively small compared to that for the H and T. This suggests that the Fe atom behaves as a classical mechanical particle.

In order to understand the detailed diffusion mechanisms at a microscopic molecular level, it would be useful to present the free-energy surface $F_T(q)$ along appropriate reaction coordinates q at temperature T.[60] The free-energy $F_T(q)$ corresponds to the reversible work to move the center-of-masses of the quantum particle to q, which is defined as $F_T(q) = -k_B T \ln \rho_T(q)$, where $\rho_T(q)$ is the nuclear distribution probability to be observed at a given set of centroid coordinates q obtained from PIMD at T. Figure 5 displays the two-dimensional free-energy surfaces at T = 300 and 500 K on the (100) plane of the bcc Fe lattice obtained from the PIMD simulations. The values shown in the figures are free-energy barriers (in eV) at the S-site and O-site (see also Figure 1). These plots are quite useful for understanding the microscopic mechanism of the H/T diffusion processes because such an energy landscape provides the means to analyze the possible diffusion pathways at the temperature of our interest. For H diffusion at T = 300 K, the quantum free-energy barrier via the S-site was estimated to be 0.042 eV (measured from the T-site), while the corresponding barrier via the O-site was obtained to be 0.058 eV (see Figure 5a). This result suggests that the H diffusion process mainly occurs via the S-site. However, it should be emphasized that one cannot ignore the contribution of the diffusion pathway via the O-site at this temperature since the energy difference between the S-site and O-site barriers is rather small. In the case of T diffusion at T = 300 K (see Figure 5b), the quantum free-energy barriers via the S-site and O-site were estimated to be 0.066 eV (measured from the T-site) and 0.099 eV (measured from the T-site), respectively. Thus, comparing the height of the barriers, we can confirm that this system clearly shows isotope effects for the H/T migration at 300 K. Besides, the free-energy barriers obtained from the classical MD simulations are much higher than those barriers obtained from the quantum simulations. This also indicates the importance of quantum effects even at room temperature. Our results are consistent with the previous CMD results of Kimizuka et al.,[18,19] although they have given one-dimensional free-energy profiles. As can be expected, the free-energy difference between the S-site and O-site barriers becomes larger as temperature increases (see Figure 5d). One of the important origins for this temperature dependence in the barrier height may be large quantum fluctuation at low temperatures, which is characterized by the radius of gyration of the ring polymer at the transition state.[17] In the case of the T diffusion processes, the corresponding energy difference becomes larger than in the case of H diffusion. In addition, the free-energy barriers for H and T diffusion obtained from the quantum mechanical simulations are always much smaller than those for H diffusion obtained from the classical MD simulations. This implies that one should employ appropriate methods that can account for nuclear quantum effects in order to discuss the diffusion dynamics of heavy tritium atoms at a quantitative level.

It may be interesting to compare the free-energy barrier of Figure 5 to the activation energy, the slope of Arrhenius plots in Figure 2. The activation energies for the H diffusion coefficients obtained from the present RPMD simulations can be roughly estimated to be 0.03 and 0.04 eV at T = 300 and 500 K, respectively. Similarly, the activation energies for the T diffusion coefficients are estimated to be 0.07 and 0.09 eV at T = 300 and 500 K, respectively. Thus, the agreement between the free-energy barriers at the S-site and the above activation energies is seen to be fairly good, although the statistical uncertainty of the RPMD simulations is somewhat large. Again, this rough agreement implies that the dominant bottleneck for the H and T diffusion processes in Fe is the S-site at least for $T \geq$ 300 K. We have also estimated imaginary vibrational frequencies along the reaction coordinate using the normal-

dx.doi.org/10.1021/jp307660e | J. Phys. Chem. C 2012, 116, 23113−23119

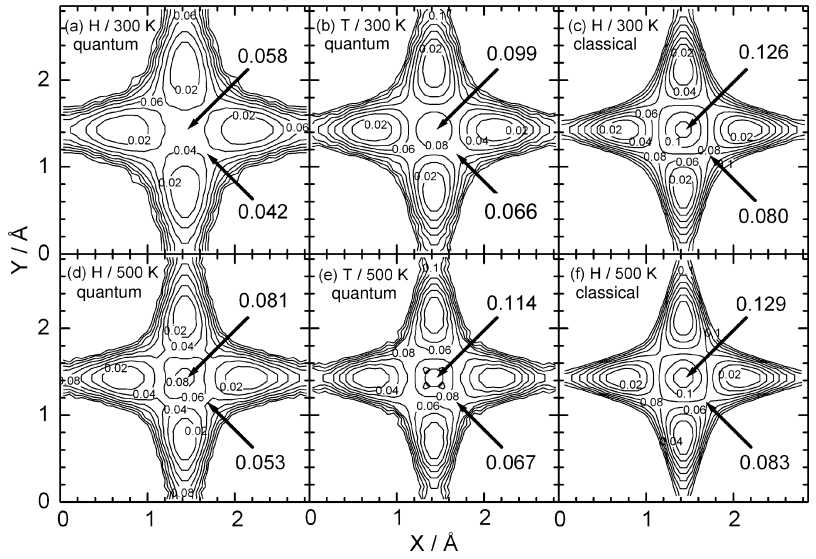

Figure 5. Two-dimensional contour plots of free-energy surfaces (in eV) as a function of the Cartesian (X,Y) coordinates (in Å) on the Fe(100) plane obtained from the static path integral molecular dynamics simulations at T = 300 and 500 K.

mode analysis on the present EAM potential. The obtained frequencies are 1460i and 810i cm^{-1} at the S-site for the Fe−H and Fe−T systems, respectively. Thus, these values can qualitatively explain the difference in the crossover temperature between H and T diffusion; the crossover temperature for H diffusion is much lower than that for T due to a larger contribution of quantum tunneling of hydrogen. However, it should mentioned that this is a very simplified picture because the diffusion pathways at lower temperatures show broader distributions, as Kimizuka et al. has already shown in their previous study.[18,19]

Finally, it will be interesting to compare the results with the centroid density QTST.[17,36−41,50,51] In Figure 6, the diffusion coefficients from CMD/RPMD are plotted as a function of $\exp(-\Delta F(T)/k_BT)$, where ΔF was estimated with the ratio between the centroid probability densities at the S-site region and the T-site region from the PIMD results. The thermal-quantum crossover temperature can be roughly estimated from these plots.[17] For example, in the case of H diffusion, we can clearly see a significant slope change at $\exp(-\Delta F(T)/k_BT) \sim 0.3$, corresponding to $T \sim 500$ K. This suggests a change in the diffusion mechanism between thermal and quantum processes around this temperature. On the other hand, in the case of T diffusion, the slope change is not so clear compared to the H case; however, we can also see a small slope change around $\exp(-\Delta F(T)/k_BT) \sim 0.08$ corresponding to $T \sim 300$ K. However, the slopes of both isotopes calculated with the classical MD method are almost constant. It should be emphasized that these crossover temperature values are consistent with Arrhenius plots of diffusion coefficients presented in Figure 2. We hope our computational result will be a stimulus to experiments, although no data have been reported so far for T diffusion.

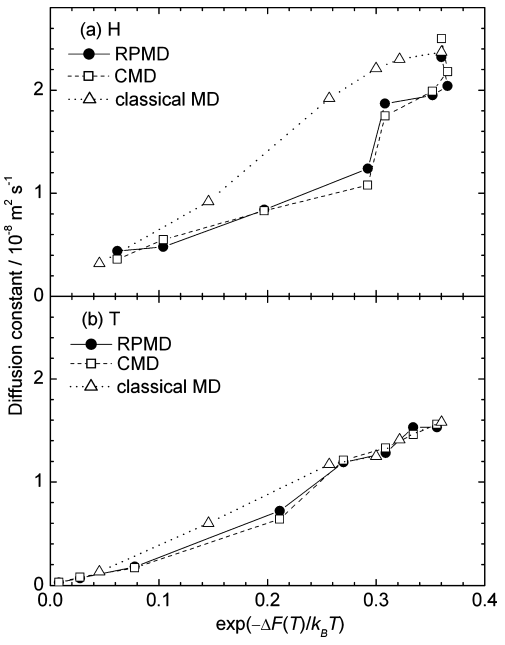

Figure 6. Plots as a function of $D(T)$ obtained from the quantum simulations and $\exp(-\Delta F(T)/k_BT)$ obtained from the free energy. The symbols and lines are same as in Figure 2. Dotted line represents the line connecting classical points.

CONCLUSIONS

In this work, we have carried out approximate quantum dynamical techniques simulations based on the CMD and RPMD methods using the EAM potential to study the H/T diffusion processes in α-Fe in the temperature range of T = 100−1000 K. It has been found that the H and T diffusion has the crossover at about T = 500 and 300 K, respectively, which implies that nuclear quantum effects are not negligible at these temperatures or lower. The result is quite similar between the CMD and RPMD methods as well as centroid density QTST based on the PIMD method, which seems to be convincing. The importance of quantum diffusion, even at the room temperature, could be a noticeable outcome that might be of help to tritium confinement problems mentioned in the Introduction.

dx.doi.org/10.1021/jp307660e | J. Phys. Chem. C 2012, 116, 23113−23119

AUTHOR INFORMATION

Corresponding Author

*E-mail: s11ds009@mail.saitama-u.ac.jp (T.Y.), tako@mail.saitama-u.ac.jp (T.T), shiga.motoyuki@jaea.go.jp (M.S).

Notes

The authors declare no competing financial interest.

ACKNOWLEDGMENTS

We would like to thank Prof. Takuji Oda in the University of Tennessee for his many helpful discussions. We also thank Grant-in-Aid for Scientific Research for the priority area 476, "Tritium for Fusion", by Ministry of Education, Culture, Sports, Science and Technology, Japan. One of the authors (M.S.) thanks the Grant-in-Aid for Scientific Research Nos. 2018024, 22750023, and 23350010. The work of H.K. is supported by Grant-in-Aid for Young Scientists (A), No. 24686072.

REFERENCES

(1) Tanabe, T. *J. Nucl. Mater.* **2011**, *417*, 545−550.
(2) Nishi, M.; Yamanishi, T.; Hayashi, T. DEMO Plant Design Team. *Fusion Eng. Des.* **2006**, *81*, 745−751.
(3) Völkl, J.; Alefeld, G. *Hydrogen in Metals I: Basic Properties*; Alefeld, G., Völkl, J., Eds.; Topics in Applied Physics Vol. 28; Springer-Verlag: Berlin, 1978; pp 321−348.
(4) Sandrock, G. *J. Alloys Comp.* **1999**, *293*−*295*, 877−888.
(5) Louthan, M. R., Jr.; Caskey, G. R., Jr.; Donovan, J. A.; Rawl, D. E., Jr. *Mater. Sci. Eng.* **1972**, *10*, 357−368.
(6) Shiga, M.; Yamaguchi, M.; Kaburaki, H. *Phys. Rev. B* **2003**, *68*, 245402.
(7) Wipf, H. *Hydrogen in Metals III: Properties and Applications*; Wipf, H., Ed.; Topics in Applied Physics Vol. 73; Springer-Verlag: Berlin, 1997; pp 51−91.
(8) Bryan, W. L.; Dodge, B. F. *AIChE J.* **1963**, *9*, 223−228.
(9) Dillard, J. L.; Seances, C. R. *Acad. Sci. Ser. C* **1970**, *270*, 669−672.
(10) Heumann, Th.; Domke, E. *Ber. Bunsen Phys. Chem.* **1972**, *76*, 825−826.
(11) Kiuchi, K.; McLellan, R. B. *Acta Metall.* **1982**, *31*, 961−984.
(12) Nagano, M.; Hayashi, Y.; Ohtani, N.; Isshiki, M.; Igaki, K. *Scripta Metall.* **1982**, *16*, 973−976.
(13) Hayashi, Y.; Hagi, H.; Tahara, A. *Z. Phys. Chem.* **1989**, *164*, 815−820.
(14) Nagano, M.; Hayashi, Y.; Ohtani, N.; Isshiki, M.; Igaki, K. *Trans. JIM* **1981**, *22*, 423−429.
(15) Hagi, H. *Mater. Trans., JIM* **1994**, *35*, 112−117.
(16) Dyer, M.; Zheang, C.; Alavi, A. *ChemPhysChem* **2005**, *6*, 1711−1715.
(17) Gillan, M. J. *Phys. Rev. Lett.* **1987**, *58*, 563−566.
(18) Kimizuka, H.; Mori, H.; Ushida, H.; Ogata, S. *J. Jpn. Inst. Met.* **2009**, *73*, 571−576.
(19) Kimizuka, H.; Mori, H.; Ogata, S. *Phys. Rev. B* **2011**, *83*, 094110.
(20) Kimizuka, H.; Ogata, S. *Phys. Rev. B* **2011**, *84*, 024116.
(21) Feynman, R. P.; Hibbs, A. R. *Quantum Mechanics and Path Integrals*; McGraw-Hill: New York, 1965.
(22) Feynman, R. P. *Statistical Mechanics*; Benjamin: New York, 1972.
(23) Chandler, D.; Wolynes, P. G. *J. Chem. Phys.* **1981**, *74*, 4078−4095.
(24) Cao, J.; Voth, G. A. *J. Chem. Phys.* **1993**, *99*, 10070−10073.
(25) Cao, J.; Voth, G. A. *J. Chem. Phys.* **1994**, *100*, 5106−5117.
(26) Cao, J.; Voth, G. A. *J. Chem. Phys.* **1994**, *101*, 6157−6167.
(27) Cao, J.; Voth, G. A. *J. Chem. Phys.* **1994**, *101*, 6168−6183.
(28) Cao, J.; Voth, G. A. *J. Chem. Phys.* **1994**, *101*, 6184−6192.
(29) Jang, S.; Voth, G. A. *J. Chem. Phys.* **1999**, *111*, 2357−2370.
(30) Jang, S.; Voth, G. A. *J. Chem. Phys.* **1999**, *111*, 2371−2384.
(31) Craig, I. R.; Manolopoulos, D. E. *J. Chem. Phys.* **2004**, *121*, 3368−3373.
(32) Craig, I. R.; Manolopoulos, D. E. *J. Chem. Phys.* **2005**, *122*, 084106.
(33) Craig, I. R.; Manolopoulos, D. E. *J. Chem. Phys.* **2005**, *123*, 034102.
(34) Braams, B. J.; Manolopoulos, D. E. *J. Chem. Phys.* **2006**, *125*, 124105.
(35) Suleimanov, Y. V. *J. Phys. Chem. C* **2012**, *116*, 11141−11153.
(36) Gillan, M. J. *J. Phys. C* **1987**, *20*, 3621−3641.
(37) Voth, G. A.; Chandler, D.; Miller, W. H. *J. Chem. Phys.* **1989**, *91*, 7749−7760.
(38) Mills, G.; Jónsson, H. *Phys. Rev. Lett.* **1994**, *72*, 1124−1127.
(39) Mills, G.; Jónsson, H.; Schenter, G. K. *Surf. Sci.* **1995**, *324*, 305−337.
(40) Truhlar, D. G.; Garrett, B. C.; Klippenstein, S. J. *J. Phys. Chem.* **1996**, *100*, 12771−12800.
(41) Shiga, M.; Fujisaki, H. *J. Chem. Phys.* **2012**, *136*, 184103.
(42) Daw, M. S.; Baskes, M. I. *Phys. Rev. Lett.* **1983**, *50*, 1285−1288.
(43) Daw, M. S.; Baskes, M. I. *Phys. Rev. B* **1984**, *29*, 6443−6453.
(44) Mendelev, M. I.; Han, S.; Srolovitz, D. J.; Ackland, G. J.; Sun, D. Y.; Asta, M. *Philos. Mag.* **2003**, *83*, 3977−3994.
(45) Angelo, J. E.; Moody, N. R.; Baskes, M. I. *Modell. Simul. Mater. Sci. Eng.* **1995**, *3*, 289−307. Baskes, M. I.; Sha, X.; Angelo, J. E.; Moody, N. R. *Modell. Simul. Mater. Sci. Eng.* **1997**, *5*, 651−652.
(46) Jiang, D. E.; Carter, E. A. *Phys. Rev. B* **2004**, *70*, 064102.
(47) Hirth, J. P. Effects of Hydrogen on the Properties of Iron and Steel; In *Metallurgical Transaction A*; Hirth, J. P., Ed.; Springer-Verlag: Berlin, 1980; Vol. *11*, pp 861−890.
(48) Pérez, A.; Tuckerman, M. E.; Müser, M. H. *J. Chem. Phys.* **2009**, *130*, 184105.
(49) Witt, A.; Ivanov, S. D.; Shiga, M.; Forbert, H.; Marx, D. *J. Chem. Phys.* **2009**, *130*, 194510.
(50) Voth, G. A. *J. Phys. Chem.* **1993**, *97*, 8365−8377.
(51) Mills, G.; Schenter, G. K.; Makarov, D. E.; Jónsson, H. *Chem. Phys. Lett.* **1997**, *278*, 91−96.
(52) Ceriotti, M.; Perrinello, M.; Markland, T. E.; Manolopoulos, D. E. *J. Chem. Phys.* **2010**, *133*, 124104.
(53) Shiga, M.; Tachikawa, M.; Miura, S. *Chem. Phys. Lett.* **2000**, *332*, 396−402.
(54) Shiga, M.; Tachikawa, M.; Miura, S. *J. Chem. Phys.* **2001**, *115*, 9149−9159.
(55) Shiga, M.; Nakayama, A. *Chem. Phys. Lett.* **2008**, *451*, 175−181.
(56) Hagi, H.; Hayasi, Y. *Trans. JIM* **1988**, *29*, 373−382.
(57) Calvo, F.; Costa, D. *J. Chem. Theory Comput.* **2010**, *6*, 508−516.
(58) Miyake, T.; Ogitsu, T.; Tsuneyuki, S. *Phys. Rev. Lett.* **1998**, *81*, 1873−1876.
(59) Herrero, C. P.; Ramírez, R. *Phys. Rev. Lett.* **2007**, *99*, 205504.
(60) Schmitt, U. W.; Voth, G. A. *J. Chem. Phys.* **1999**, *111*, 9361−9380.